Hybrid magnon-atom entanglement and magnon blockade via quantum interference

Fei Wang,[1] Chengdeng Gou,[2] Jun Xu,[2,*] and Cheng Gong[2,†]
[1]*School of Science, Hubei University of Technology, Wuhan 430068, China*
[2]*College of Physical Science and Technology, Central China Normal University, Wuhan 430079, China*

(Received 23 December 2021; accepted 27 June 2022; published 11 July 2022)

In this paper, we propose a quantum interference mediated control of switching between magnon-atom entanglement and magnon blockade. A three-level Λ configuration atomic ensemble and a yttrium iron garnet sphere are simultaneously coupled to a microwave cavity mode through magnetic dipole interaction. By applying two strong fields to drive the atoms, the resonant coupling between a dressed-state atomic transition and the magnon mode, without direct interaction, is established by adiabatically eliminating the cavity field. Interestingly, the anti-Jaynes-Cummings (JC) interaction and the JC interaction are alternatively formed when the atoms are trapped into different superposition states induced by quantum interference, causing the appearance of hybrid magnon-atom entanglement and magnon quantum blockade, respectively. The coherent-controlled hybrid magnon-atom entanglement and magnon blockade may find potential applications in quantum information processing.

DOI: 10.1103/PhysRevA.106.013705

I. INTRODUCTION

In recent years, the magnon-photon strong and ultrastrong coupling in microwave and optical frequency region has attracted increasing interest since it provides a promising platform for studying magnon quantum electrodynamics [1–10]. The magnon, as an example, is regarded as the quanta of collective spin excitations in yttrium iron garnet (YIG) possessing unique properties of high spin density and low damping rate [11]. Thanks to various coupling schemes involving magnetic dipole interaction, magnetostriction, and magnetic-optical coupling, one can implement the interactions between ferrimagnetic crystals and different physical systems in diversity. This brings forth new ideas to construct a variety of hybrid systems including cavity optomagnonics [12–14], cavity magnomechanics [15,16], and hybrid ferromagnetic-superconducting systems [17–19]. Up to now, the cavity-magnon system has been widely used to explore abundant macroscopic quantum effects, such as the observation of nonlinear bistability [20], magnon Kerr effect [21,22], magnon-induced transparency [23,24], nonreciprocity [25,26], slow light [27,28], and so on.

Interestingly, a large number of hybrid systems have been suggested to study the magnon squeezing [29], magnon-magnon entanglement [21], Bell state [30], and magnon Schrödinger cat state [31,32]. For instance, Li *et al.* showed that the genuine tripartite entanglement can be achieved between magnons, cavity microwave photons, and phonons in cavity magnomechanics [33], wherein the cavity photons and magnons are coupled by magnetic dipole interaction while the magnons and phonons via magnetostrictive interaction. The entanglement in this hybrid system is mainly determined by two physical processes: (i) the cavity-magnon beam splitter interaction; (ii) the magnon-phonon parametric interaction. The entanglement is basically dependent on the magnon-phonon coupling (parametric interaction), without which not only tripartite entanglement but also bipartite entanglement is absent. More recently, Kong *et al.* proposed a new scheme to prepare remote magnon entanglement based on the dispersive interactions [34]. In their work, two magnon modes are separately placed into two different microwave cavities, in which a single superconduction atom interacts simultaneously with the two cavity modes. When the cavity modes are turned to be far detuned with the superconducting atom and magnon modes, a two-channel interaction is established by virtual photon exchange, resulting in the appearance of original magnon-magnon Einstein-Podolsky-Rosen (EPR) entanglement. In fact, both the Jaynes-Cummings (JC) [35,36] and anti-JC interactions are coexistent between magnons and atomic spins in the dressed-state interaction. This is similar to the physical processes found in magnon-photon-phonon hybrid system [33]. While the magnon mode interacts with the atomic spin in an anti-JC interaction, the two-mode squeezing between the magnon and atom is created. After that, the quantum state would be transferred from atomic spin to the other magnon mode via a JC interaction, thus giving rise to the remote magnon-magnon entanglement. This provides a basic idea to prepare entanglement between distant parties. Accordingly, the magnon-magnon entanglement in their work is essentially originated from the anti-JC interaction.

On the other hand, the magnon quantum blockade, as defined, is a counterpart of photon blockade effects [37,38], namely, the absorption of the first photon would lead to the inhibition of the second and subsequent ones. The photon blockade is closely related to antibunching behavior and opens up a way to prepare a single-photon source [39,40]. Therefore,

*junxu@ccnu.edu.cn.
†gongcheng@ccnu.edu.cn

it has been extensively studied in various systems including optomechanical systems [41], coupled atom-cavity systems [42], and cavity quantum electrodynamics [43]. Recently, the strong coupling between the magnon and the superconducting qubit has been realized in experiment [17–19], which motivates researchers to pay special attention to the magnon blockade. The magnon blockade is usually divided into two categories: one is originated from anharmonicity created by strong magnon-qubit coupling, i.e., conventional magnon blockade (CMB); the other is based on the destructive quantum interference between several direct or indirect pathways in weak coupling cases, i.e., unconventional magnon blockade (UCMB). Recently, CMB [44] and UCMB [45,46] have been investigated in a hybrid ferromagnet-superconductor quantum system, respectively. Subsequently, the simultaneous blockade of a photon, phonon, and magnon induced by a two-level atom [47], and the phase-controlled multimagnon blockade and magnon-induced tunneling [48] are also achieved theoretically. In these schemes, it is found that the JC interaction between magnon and superconducting qubit is the key to generate the magnon blockade effect.

As is well known, the atomic coherence and quantum interference play an important role in controlling the optical properties of the interacting medium, causing a large number of phenomena such as coherent population trapping (CPT) and electromagnetically induced transparency (EIT), which could find potential applications in light information storage, readout and transfer [49]. More interestingly, it has been studied extensively that the coherent control of two-photon processes and dissipation scheme can be used to generate entangled and squeezed states [50,51], which are important resources for quantum teleportation [52], quantum dense coding [53], and universal quantum computation [54]. As proposed in the pioneering work by Agarwal [55], the quantum interference effects in the spontaneous emission should be taken into account if the near degenerate levels in multilevel systems are coupled by the same vacuum modes. After that, a great deal of interest has been paid on this type of quantum interference to study ultranarrow lines [56], spontaneous emission cancellation [57], quantum entanglement [58], lasing without inversion [59], etc. Generally, the spontaneously generated coherence (SGC) effects have been frequently studied in V-type atoms, while such effects have been relatively paid less attention in the Λ-type systems in spite of it was first predicted by Javananien in 1992 [60]. However, Menon and Agarwal have investigated the typical quantum interference in the Λ-type systems, finding that the SGC has remarkable effects in modifying the line profiles [61]. Subsequently, the SGC in Λ system received great interest to study the inversionless gain [62], optical bistability [63], resonance fluorescence [64], and squeezing spectra [65]. What is more, Dutt *et al.* studied the SGC effects in experiment by utilizing an artificial atomic system with Λ-type structure [66]. More recently, the long-lived spontaneously generated coherence has been generated by incoherent light and the possible experiment proposal has also been suggested [67,68].

In this paper, we present a scheme to realize the switching of quantum entanglement and magnon blockade mediated by quantum interference in a hybrid magnon-cavity-atom system. Being different from previous schemes [44–48], two strong fields are applied to resonantly drive the atomic system. The indirect interaction between the magnons and atoms is established via exchange of virtual photons in dispersive microwave cavity. Interestingly, the anti-JC interaction and JC interaction are alternatively generated when the atoms are trapped into different superposition state in dress-state picture. If an anti-JC interaction is established, the hybrid magnon-atom entanglement is generated at steady state by treating the dressed atomic spin as a bosonic mode under Holstein-Primakoff approximation. On the other hand, the CMB and UCMB are possible to attain when a JC interaction of magnon and atom is formed. The main innovative points in our scheme are summarized briefly as follows: (i) the coherent coupling between the magnon and atoms is realized by adiabatically eliminating the cavity mode; (ii) the alternative appearance of anti-JC- and JC-type interaction is determined by the quantum interference; (iii) the hybrid magnon-atom entanglement and magnon blockade can be effectively controlled by the atomic coherence.

The remaining part of the present paper is organized as follows. In Sec. II, we describe the model that consists of a Λ-type system and a YIG sphere in a microwave cavity. In Sec. III we demonstrate the generation of hybrid magnon-atom entanglement and squeezing. In Sec. IV, we discuss the analytical results for CMB and UCMB and the internal mechanisms are also analyzed in detail. Finally, the conclusion is given in Sec. V.

II. MODEL AND EQUATIONS

As sketched in Fig. 1, an atomic ensemble with Λ-type and a YIG sphere are placed into a microwave cavity, in which the cavity mode a is coupled with the transition $|g_2\rangle \leftrightarrow |g_1\rangle$ and, simultaneously interacts with the magnon mode of a YIG sphere with frequency ω_m. Both the atoms and the YIG sphere are in the yz plane, and at the wave crest of the microwave field. For the Λ-type atomic system, we apply a control field Ω_c and a strong microwave field Ω_m to resonantly drive the corresponding transitions $|e\rangle \leftrightarrow |g_2\rangle$ and $|g_2\rangle \leftrightarrow |g_1\rangle$, respectively.

The master equation for the density operator ρ of the composite magnon-cavity-atom hybrid system is written in an appropriate rotating frame as ($\hbar = 1$) [69,70]

$$\dot{\rho} = -i[H, \rho] + \mathcal{L}_c\rho + \mathcal{L}_m\rho + \mathcal{L}_a\rho \tag{1}$$

with the total system Hamiltonian

$$H = H_d + H_I, \tag{2}$$

where the first term

$$H_d = \Omega_m\sigma_{g_1g_2} + \Omega_c\sigma_{g_2e} + \text{ H.c.}, \tag{3}$$

represents the resonant interaction of the atom with the classical dressing fields, and the second term

$$H_I = g_a a\sigma_{g_2g_1}e^{i\delta t} + g_m am^\dagger e^{i\Delta t} + \text{ H.c.} \tag{4}$$

describes the simultaneous interaction of the cavity field with the atom and magnon mode. Here $\sigma_{lm} = \sum_{\mu=1}^{N} |l_\mu\rangle\langle m_\mu|(l, m = g_1, g_2, e)$ are the projection operators of N independent atoms for $l = m$ and the flip operators for $l \neq m$. a ($a^\dagger$) and m ($m^\dagger$) are the annihilation (creation)

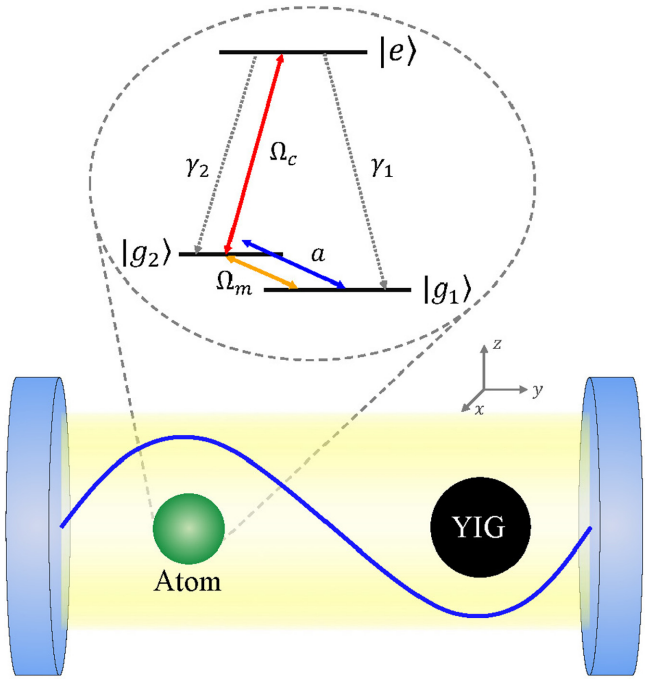

FIG. 1. (a) Schematic diagram of the magnon-atom system. A ferromagnetic YIG sphere and a three-level Λ-type atomic ensemble are installed in a microwave cavity. A control field Ω_c and a microwave field Ω_m are applied to resonantly drive the corresponding transitions $|e\rangle \leftrightarrow |g_2\rangle$ and $|g_2\rangle \leftrightarrow |g_1\rangle$, respectively. A microwave quantized field mode a is coupled with the transition $|g_2\rangle \leftrightarrow |g_1\rangle$ and, at the same time, with the magnon mode of a YIG sphere with frequency ω_m.

operator for the cavity field and magnon mode. g_a and g_m are the coupling strength of interaction of the cavity field with the atoms and the magnon. $\delta = \omega_{g_2g_1} - \nu$ and $\Delta = \omega_m - \nu$ are the detunings of the atomic transition frequency $\omega_{g_2g_1}$ and the magnon frequency ω_m from the cavity field frequency ν. The damping of the cavity field $\mathcal{L}_c\rho$, the magnon mode damping $\mathcal{L}_m\rho$, and the atomic decay between different atomic states denoted by $\mathcal{L}_a\rho$ are described as follows:

$$\mathcal{L}_c\rho = \frac{\kappa_a}{2}(2a\rho a^\dagger - \rho a^\dagger a - a^\dagger a\rho), \tag{5}$$

$$\mathcal{L}_m\rho = \frac{\kappa_m}{2}(2m\rho m^\dagger - \rho m^\dagger m - m^\dagger m\rho), \tag{6}$$

$$\begin{aligned}\mathcal{L}_a\rho = &\sum_{j=1}^{2}\frac{\gamma_j}{2}(2\sigma_{g_je}\rho\sigma_{eg_j} - \sigma_{ee}\rho - \rho\sigma_{ee}) \\ &+ \frac{\gamma_p}{4}(2\sigma_p\rho\sigma_p - \sigma_p\sigma_p\rho - \rho\sigma_p\sigma_p) \\ &+ \gamma_{12}\sigma_{g_1e}\rho\sigma_{eg_2} + \gamma_{21}\sigma_{g_2e}\rho\sigma_{eg_1},\end{aligned} \tag{7}$$

wherein κ_a, κ_m, and γ_j are the damping rates of the cavity, the magnon, and the corresponding atomic transitions. γ_p is the dephasing rate between the two lower levels and $\sigma_p = \sigma_{g_2g_2} - \sigma_{g_1g_1}$. $\gamma_{12} = \gamma_{21} = \beta\sqrt{\gamma_1\gamma_2}$ represents the spontaneously generated coherence (SGC) effect [55] due to the cross coupling between the two decay paths $|e\rangle \to |g_1\rangle$ and $|e\rangle \to |g_2\rangle$, among which the parameter $\beta = \frac{\vec{\mu}_{eg_1}\cdot\vec{\mu}_{eg_2}}{|\vec{\mu}_{eg_1}||\vec{\mu}_{eg_2}|}$ stands for the alignment of the two dipole moments $\vec{\mu}_{eg_1}$ and $\vec{\mu}_{eg_2}$. The SGC tends to vanish, i.e., $\beta = 0$, when the two dipole moments are orthogonal. However, the SGC effect is maximal for $\beta = \pm 1$ corresponding to the cases that they are parallel or antiparallel.

To describe clearly the physical mechanisms, we resort to the dressed atomic picture by diagonalizing the Hamiltonian H_d under the conditions of $\Omega_{c,m} \gg \gamma_j, \kappa_{a,m}, g_{a,m}$. The dressed atomic states are expressed in terms of bare states as [71]

$$\begin{aligned}|\tilde{0}\rangle &= -\sin\theta|g_1\rangle + \cos\theta|e\rangle, \\ |\tilde{1}\rangle &= \frac{1}{\sqrt{2}}(\cos\theta|g_1\rangle - |g_2\rangle + \sin\theta|e\rangle), \\ |\tilde{2}\rangle &= \frac{1}{\sqrt{2}}(\cos\theta|g_1\rangle + |g_2\rangle + \sin\theta|e\rangle)\end{aligned} \tag{8}$$

with $\sin\theta = \frac{\Omega_c}{\tilde{\Omega}}$, $\cos\theta = \frac{\Omega_m}{\tilde{\Omega}}$, and $\tilde{\Omega} = \sqrt{\Omega_c^2 + \Omega_m^2}$. The dressed states $|\tilde{0}\rangle$, $|\tilde{1}\rangle$, and $|\tilde{2}\rangle$ have their eigenvalues 0, $-\tilde{\Omega}$, and $\tilde{\Omega}$, respectively. It means that the spacings between these dressed states are identical. Now the interaction Hamiltonian H_d becomes the diagonal form in the dressed-state picture

$$\tilde{H}_d = \tilde{\Omega}(\sigma_{\tilde{2}\tilde{2}} - \sigma_{\tilde{1}\tilde{1}}), \tag{9}$$

where $\sigma_{\tilde{k}\tilde{l}} = \sum_{\mu=1}^{N}|\tilde{k}_\mu\rangle\langle\tilde{l}_\mu|(k, l = 0, 1, 2)$ are the projection operators ($k = l$) and the flip operators ($k \neq l$) of the ensemble in terms of the dressed states. By transforming the bare atomic relaxation terms into the dressed-state picture and neglecting the quantized modes temporarily, we can obtain the steady-state populations of the dressed states $N_k = \langle\sigma_{\tilde{k}\tilde{k}}\rangle$, which is given in Appendix.

It is assumed that the atomic system with Λ-type are trapped into a small trapping volume [72]. In the following numerical calculations, we always set $\gamma_1 = \gamma_2 = \gamma$ and $\Omega_{c,m} \gg \gamma \gg \gamma_p$, which is always justified in atomic or atom-like systems [66,73]. Taking ^{87}Rb atom as an example, the atomic relaxation rate of $\gamma_{1,2}$ are usually of the order MHz. As proposed in Ref. [73], the Rabi frequencies of the driving fields $\Omega_{c,m}$ can reach the values of the order GHz even THz, satisfying the conditions of $\Omega_{c,m} \gg \gamma$. Furthermore, the dephasing rate γ_p between the two ground states is of the order KHz [74]. Therefore, without loss of generality, the other parameters are assumed to be scaled in units of γ.

Figures 2(a) and 2(b) plot the normalized steady-state populations of the dressed states $\bar{N}_k = N_k/N$ versus the amplitude ratio Ω_c/Ω_m for parallel and antiparallel dipole moments by taking $\gamma_p = 0$, respectively. Clearly, for $\beta = 1$, the normalized dressed-state population of $\bar{N}_2$ drops slowly from 1 while $\bar{N}_1$ increases slightly from 0 with the increasing of the ratio Ω_c/Ω_m. In the region of $0 < \Omega_c/\Omega_m \leqslant 0.5$, it is seen that all of the dressed-state populations almost keep unchanged. Notably, the evolutions of $\bar{N}_2$ and $\bar{N}_1$ versus Ω_c/Ω_m are completely conversed for $\beta = -1$. In addition, it is found that the variation trends for $\bar{N}_0$ are the same in the two cases. Specifically, at $\Omega_c/\Omega_m = 0.5$ for $\beta = 1$, we have $\bar{N}_2 = 0.983$, $\bar{N}_1 = 0.003$, and $\bar{N}_0 = 0.014$, implying that the atoms are nearly trapped into the superposition state $|\tilde{2}\rangle$, as shown in Fig. 2(a). This is the well-known coherent population trapping (CPT) effect. Oppositely, the dressed-state population would be trapped into the state $|\tilde{1}\rangle$ in the region of $0 < \Omega_c/\Omega_m \leqslant 0.5$ for $\beta = -1$ as shown in Fig. 2(b). When $\gamma_p = 0.01\gamma$ and

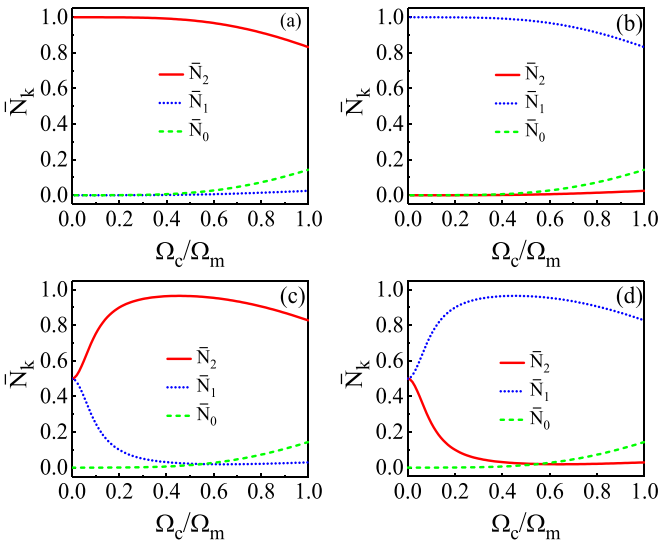

FIG. 2. The steady-state normalized populations of the dressed states $\bar{N}_k$ versus the amplitude ratio Ω_c/Ω_m. Taking parameters $\gamma_{1,2} = \gamma$ and (a) $\gamma_p = 0, \beta = 1$; (b) $\gamma_p = 0, \beta = -1$; (c) $\gamma_p = 0.01\gamma$, $\beta = 1$; (d) $\gamma_p = 0.01\gamma$, $\beta = -1$.

$\beta = 1$, $\bar{N}_2$ first increases rapidly from 0.5 and then decreases rapidly with the increasing of Ω_c/Ω_m, while $\bar{N}_1$ first decreases rapidly from 0.5 and then increases slowly. The dressed-state population would be nearly trapped into the state $|\tilde{2}\rangle$ in the region of $0.3 \leqslant \Omega_c/\Omega_m \leqslant 0.62$ ($\bar{N}_2 \geqslant 0.95$), as shown in Fig. 2(c). Likewise, the dressed-state population would be trapped into the state $|\tilde{1}\rangle$ in the region of $0.3 \leqslant \Omega_c/\Omega_m \leqslant 0.62$ for $\beta = -1$, as shown in Fig. 2(d). It is seen that the atomic coherence induced by the strong driven fields and quantum interference effects are combined to create the population trapping and population conversion. In addition, it is noted that the dephasing rate γ_p has an evident effect on modifying the evolution of dressed-state population.

By expressing the interaction Hamiltonian (4) based on dressed states, making a further unitary transformation to H_I with $U = \exp(-i\tilde{H}_d t)$, i.e., $UH_IU^\dagger$ and assuming $|\delta|, |\delta \pm \tilde{\Omega}|, |\delta - 2\tilde{\Omega}| \gg |\delta + 2\tilde{\Omega}|$, the interaction Hamiltonian can be written as

$$\tilde{H}_I = \frac{g_a \cos\theta}{2} a\sigma_{\tilde{2}\tilde{1}} e^{i(\delta+2\tilde{\Omega})t} + g_m a m^\dagger e^{i\Delta t} + \text{H.c.} \quad (10)$$

Here we have tuned the magnon mode being resonant with the second-order Rabi sideband, i.e., $\omega_m = \omega_{g_2 g_1} + 2\tilde{\Omega}$ or $\Delta = \delta + 2\tilde{\Omega}$, but the cavity field being far detuned from the second-order Rabi sideband. By assuming the cavity field decays much more rapidly than the atom and the magnon mode, we can adiabatically eliminate the cavity mode. Following the technique as in Ref. [75], the effective interaction Hamiltonian can be derived as

$$H_{\text{eff}} = -i\tilde{H}_I(t) \int dt' \tilde{H}_I(t'). \quad (11)$$

Discarding the rapidly oscillating terms, we obtain the effective interaction Hamiltonian

$$H_{\text{eff}} = \frac{g\cos\theta}{2}(m\sigma_{\tilde{2}\tilde{1}} + \sigma_{\tilde{1}\tilde{2}} m^\dagger), \quad (12)$$

where the effective coupling strength is defined as $g = \frac{g_a g_m}{\Delta}$. It is seen from the above effective Hamiltonian that the coherent coupling between atoms and magnon mode, although without direct interaction, is established effectively. This is based on the simultaneous interactions of the magnon and the atoms with the cavity field. The cavity field is tuned to be far detuned from the atomic second-order Rabi sideband and the magnon mode frequency, and then it can be adiabatically eliminated. In short, the strong fields are used to establish the atomic coherence and the microwave cavity mode is to create effective interaction of magnon and atoms via virtual photon exchange.

III. HYBRID MAGNON-ATOM ENTANGLEMENT AND SQUEEZING

Now we are in a position to investigate the quantum effects in the hybrid system. First, the maximal quantum interference is considered when two atomic dipole moments $\vec{\mu}_{eg_1}$ and $\vec{\mu}_{eg_2}$ are parallel, i.e., $\beta = 1$. At this time, it is clear that the population of the dressed state $|\tilde{2}\rangle$ is greater than that of the dressed state $|\tilde{1}\rangle$, i.e., $N_2 > N_1$. Under such condition, we can adopt the Holstein-Primakoff approximation [76] to describe the atomic ensemble as a bosonic field, i.e., $c = \sigma_{\tilde{2}\tilde{1}}/\sqrt{N_2 - N_1}$ satisfying $[c, c^\dagger] = 1$. By defining the parameter $\xi = \frac{g\cos\theta}{2}\sqrt{N_2 - N_1}$, the system effective Hamiltonian can be rewritten as

$$H_{\text{eff}} = \xi m c + \xi c^\dagger m^\dagger, \quad (13)$$

which represents the anti-JC-type interaction between the magnon and atom, being similar to the parametric interaction.

To investigate the quantum correlations between atoms and magnon modes, following the standard technique, we derive a set of linearized quantum Langevin equations (QLEs) as follows [77]:

$$\begin{aligned} \dot{m} &= -\frac{\kappa_m}{2} m - i\xi c^\dagger + \sqrt{\kappa_m} F_m(t), \\ \dot{c} &= -\frac{\Gamma}{2} c - i\xi m^\dagger + \sqrt{\Gamma} F_c(t), \end{aligned} \quad (14)$$

wherein Γ represents the decay rate of the spin down flip operator, which is given in Appendix. It is noted that the symbol δ is omitted from now on because the expectation values of these operators are equal to zero in our schemes, i.e., $\langle \hat{O} \rangle = 0$. The noise operators satisfy the nonzero correlations $\langle F_m(t) F_{m^\dagger}(t') \rangle = (n_{\text{th}} + 1)\delta(t - t')$, $\langle F_{m^\dagger}(t) F_m(t') \rangle = n_{\text{th}}\delta(t - t')$, $\langle F_{c^\dagger}(t) F_c(t') \rangle = \frac{N_1}{N_2 - N_1}\delta(t - t')$, $\langle F_c(t) F_{c^\dagger}(t') \rangle = \frac{N_2}{N_2 - N_1}\delta(t - t')$. Here $n_{\text{th}} = (e^{\hbar\omega_m/k_B T} - 1)$ is the mean magnon number of thermal excitations at the magnon frequency ω_m, in which k_B is the Boltzmann constant and T is the bath temperature. It should be pointed out that in order to consider the influence of temperature on the following mentioned quantum effects, an absolute value rather than a relative value of ω_m should be given. As proposed in Ref. [45], the magnon frequency is set as $\omega_m/2\pi = 6.5$ GHz, which is possible to match the condition of $\omega_m = \omega_{g_2 g_1} + 2\tilde{\Omega}$.

The above QLEs can be written in the quadrature form, with quadrature fluctuations defined as $X = (m + m^\dagger)/\sqrt{2}$, $Y = i(m^\dagger - m)/\sqrt{2}$, $x = (c + c^\dagger)/\sqrt{2}$, $y = i(c^\dagger - c)/\sqrt{2}$ (similar definition for noises F_X, F_Y, F_x, F_y), which are

written as

$$\dot{X} = -\frac{\kappa_m}{2}X - \xi y + \sqrt{\kappa_m}F_X(t),$$
$$\dot{Y} = -\frac{\kappa_m}{2}Y - \xi x + \sqrt{\kappa_m}F_Y(t),$$
$$\dot{x} = -\frac{\Gamma}{2}x - \xi Y + \sqrt{\Gamma}F_x(t),$$
$$\dot{y} = -\frac{\Gamma}{2}y - \xi X + \sqrt{\Gamma}F_y(t). \quad (15)$$

They can be cast in the matrix form

$$\dot{u}(t) = Au(t) + n(t), \quad (16)$$

where $u(t) = (X, Y, x, y)^T$, A is the drift matrix

$$A = \begin{pmatrix} -\frac{\kappa_m}{2} & 0 & 0 & -\xi \\ 0 & -\frac{\kappa_m}{2} & -\xi & 0 \\ 0 & -\xi & -\frac{\Gamma}{2} & 0 \\ -\xi & 0 & 0 & -\frac{\Gamma}{2} \end{pmatrix}, \quad (17)$$

and $n(t) = (\sqrt{\kappa_m}F_X, \sqrt{\kappa_m}F_Y, \sqrt{\Gamma}F_x, \sqrt{\Gamma}F_y)^T$. The system is stable only if all eigenvalues of the drift matrix A have negative real parts, which can be derived from the Routh-Hurwitz criterion [78],

$$\lambda_\pm = \frac{1}{4}[-(\kappa_m + \Gamma) \pm \sqrt{(\kappa_m + \Gamma)^2 - 4(\kappa_m\Gamma - 4\xi^2)}]. \quad (18)$$

Since the dynamics of the system is linear and the input noises are Gaussian, the dynamical map preserves the Gaussian nature of any input state. The steady state of quantum fluctuations of the system is therefore a continuous variable two-mode Gaussian state, which is completely characterized by an 4×4 covariance matrix (CM) V, defined as $V_{ij}(t) = \langle u_i(t)u_j(t') + u_j(t')u_i(t)\rangle/2$. When the system is stable, $t \to \infty$, the solution of V can be obtained by directly solving the Lyapunov equation [79]

$$AV + VA = -D, \quad (19)$$

where D is the diffuse matrix defined by $D_{ij}\delta(t - t') = \langle n_i(t)n_j(t') + n_j(t')n_i(t)\rangle/2$, given as

$$D = \begin{pmatrix} \kappa_m\left(n_{\rm th} + \frac{1}{2}\right) & 0 & 0 & 0 \\ 0 & \kappa_m\left(n_{\rm th} + \frac{1}{2}\right) & 0 & 0 \\ 0 & 0 & \frac{\Gamma N_+}{2N_-} & 0 \\ 0 & 0 & 0 & \frac{\Gamma N_+}{2N_-} \end{pmatrix}, \quad (20)$$

wherein $N_\pm = N_2 \pm N_1$. Once the CM of the system is achieved, one can then calculate the degree of the hybrid magnon-atom entanglement.

Here, we use the logarithmic negativity E_N to quantify the degree of entanglement. This quantity is a rigorous entanglement monotone, and is zero for separable states. For two-mode Gaussian states in our system, it can be calculated using the expression [80,81]

$$E_N \equiv \max[0, -\ln 2\tilde{v}_-], \quad (21)$$

where $\tilde{v}_- = \min \text{eig}|i\Omega_2\tilde{V}|$ (with the symplectic matrix $\Omega_2 = \oplus_{j=1}^2 i\sigma_y$ and the y-Pauli matrix σ_y) is the minimum symplectic eigenvalue of the CM $\tilde{V} = \mathcal{P}_{1|2}V\mathcal{P}_{1|2}$, where $\mathcal{P}_{1|2} = \text{diag}(1, -1, 1, 1)$ is the matrix that implements partial transposition at the level of CMs.

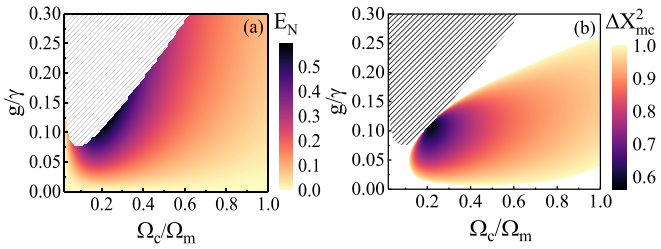

FIG. 3. Density plot of (a) hybrid magnon-atom entanglement E_N and (b) hybrid magnon-atom squeezing ΔX^2_{mc} versus the amplitude ratio Ω_c/Ω_m and the coupling strength g/γ. The parameters are chosen as $\gamma_{1,2} = \gamma$, $\gamma_p = 0.01\gamma$, $\beta = 1$, $\kappa_m = 0.1\gamma$. The shadow region shows the unstable region, and the empty region in (b) represents the areas where squeezing is greater than 1.

In addition, by defining a pair of quadrature operators as $X_{mc} = X + y$ and $P_{mc} = Y - x$, the two-mode squeezing occurs if the following inequalities are satisfied [69,70]:

$$\Delta X^2_{mc} < 1, \quad \text{or} \quad \Delta P^2_{mc} < 1. \quad (22)$$

According to the QLEs, we can analytically derived the variance of two-mode squeezing ΔX^2_{mc}.

$$\Delta X^2_{mc} = \frac{\kappa_m\Gamma(\kappa_m + \Gamma - 4|\xi|)}{(\kappa_m + \Gamma)(\kappa_m\Gamma - 4|\xi|^2)}\frac{N_2}{N_2 - N_1}. \quad (23)$$

In Fig. 3, we show the density plot of the hybrid magnon-atom entanglement E_N and squeezing ΔX^2_{mc} versus the amplitude ratio Ω_c/Ω_m and the coupling constant g/γ by taking $\gamma_{1,2} = \gamma$, $\gamma_p = 0.01\gamma$, $\beta = 1$, $\kappa_m = 0.1\gamma$. In Fig. 4, we give the density plot of E_N and ΔX^2_{mc} versus γ_p/γ and Ω_c/Ω_m by choosing $g = 0.1\gamma$. First, as shown in Fig. 3, it is seen that the magnon-atom entanglement and squeezing happen in some regions. It is reasonable that the effective coupling parameter ξ is a key factor to determine the entanglement and squeezing. To show this, we plot the evolution of ξ/γ and Γ/γ as a function of Ω_c/Ω_m in Figs. 5(a) and 5(b), respectively. We find that as $\gamma_p = 0$, the parameter ξ falls monotonously with the increasing of Ω_c/Ω_m. While for $\gamma_p \neq 0$, we see that the parameter ξ increases first to a maximal value and then decreases slowly. This would lead to the similar evolution of

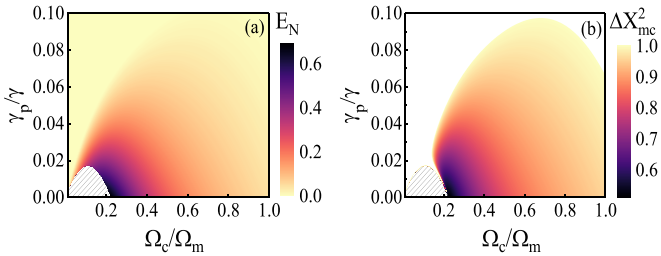

FIG. 4. Density plot of (a) hybrid magnon-atom entanglement E_N and (b) hybrid magnon-atom squeezing ΔX^2_{mc} versus the amplitude ratio Ω_c/Ω_m and the dephasing rate γ_p/γ. Taking $g = 0.1\gamma$ and the other parameters are the same as in Fig. 3. The shadow and empty regions represent the same meanings as in Fig. 3.

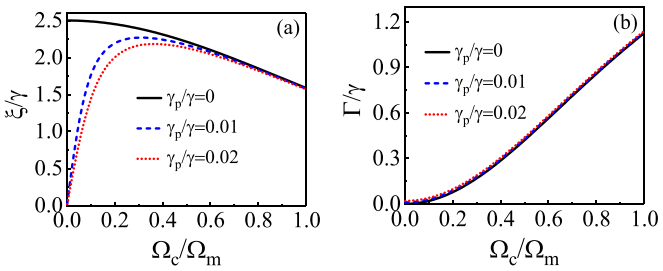

FIG. 5. (a) The effective coupling constant ξ/γ and (b) decay rate Γ/γ as a function of the amplitude ratio Ω_c/Ω_m for $\gamma_p = 0$ (solid line), $\gamma_p = 0.01\gamma$ (dashed line), $\gamma_p = 0.02\gamma$ (dotted line). The parameters are taken as $\gamma_{1,2} = \gamma$, $\beta = 1$, $g = 5\gamma$.

the entanglement and squeezing, as shown in Fig. 3. Moreover, the entanglement and squeezing can be achieved in the weak coupling cases, and the degrees of entanglement and squeezing are enhanced with the increasing of coupling constant g. In the present scheme, the two-mode entanglement and squeezing are strongly dependent on the dressed-state population difference $N_2 - N_1$, which is essentially determined by the quantum interference β and the amplitude ratio Ω_c/Ω_m. Once the coherent coupling of magnon and atom is established by virtual photon exchange, the hybrid magnon-atom entanglement and squeezing are obtainable under appropriate conditions.

Furthermore, as shown in Fig. 4, the dephasing rate γ_p between the two ground states $|g_1\rangle$ and $|g_2\rangle$ has a remarkable influence on the hybrid atom-magnon entanglement and squeezing. As the increase of γ_p, the entanglement E_N and the squeezing ΔX^2_{mc} disappear gradually, which can be attributed to the fact that the CPT effect is spoiled by the dephasing rate, which can be seen in Figs. 2(c) and 2(d). Nevertheless, the increase of γ_p is beneficial to the stability of the system. In addition, the magnon-atom entanglement and squeezing are robust against environmental temperature for different dephasing rates, as shown in Fig. 6. It can be seen that the entanglement and squeezing will disappear when temperature exceeds about 450 mK for the case of $\gamma_p = 0$. With the increase of the dephasing rate, the temperature tolerance of entanglement and squeezing will decrease. However, the entanglement and squeezing are relatively stable in the temperature range of 0–100 mk.

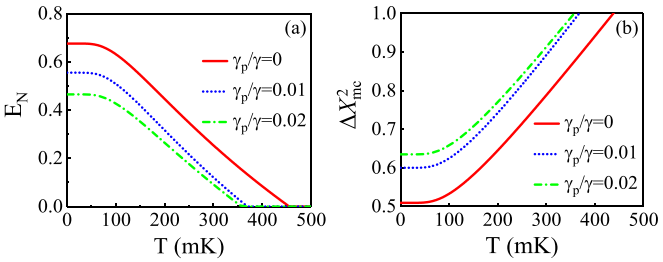

FIG. 6. (a) E_N and (b) ΔX^2_{mc} versus temperature T for $\gamma_p = 0$, $g = 0.1\gamma$, $\Omega_c/\Omega_m = 0.23$ (solid line), $\gamma_p = 0.01\gamma$, $g = 0.1\gamma$, $\Omega_c/\Omega_m = 0.2$ (dotted line), $\gamma_p = 0.02\gamma$, $g = 0.12\gamma$, $\Omega_c/\Omega_m = 0.2$ (dashed line). Taking $\omega_m/2\pi = 6.5$ GHz and the other parameters are the same as in Fig. 3.

IV. CONVENTIONAL AND UNCONVENTIONAL MAGNON BLOCKADE

Next, we would like to turn to the other case of $\beta = -1$. In this case, we find that the population of the dressed state $|\tilde{1}\rangle$ is far greater than that of the dressed state $|\tilde{2}\rangle$, i.e., $N_1 \gg N_2$, in the region of $0.3 \leqslant \Omega_c/\Omega_m \leqslant 0.62$. In this case, the atoms are almost trapped into the superposition state $|\tilde{1}\rangle$. Similarly, we can define the spin down flip operator as $\tilde{c} = \sigma_{\tilde{1}\tilde{2}}/\sqrt{N_1 - N_2}$. Then the effective Hamiltonian can be rewritten as

$$\tilde{H}_{\text{eff}} = \tilde{\xi} m \tilde{c}^\dagger + \tilde{\xi} \tilde{c} m^\dagger, \tag{24}$$

represents the JC-type interaction [35] with $\tilde{\xi} = \frac{g\cos\theta}{2}\sqrt{N_1 - N_2}$. This motivates us to investigate the quantum blockade effect in present scheme.

For the observation of magnon blockade effect, we consider a weak probe field with the Hamiltonian $H_d = \Omega_d(m^\dagger e^{-i\omega_d t} + m e^{i\omega_d t})$ (with frequency ω_d and strength Ω_d) applied into the YIG sphere after returning to the original rotating frame. The effective Hamiltonian of this hybrid magnon-atom system in the appropriate rotating frame can be written as

$$\begin{aligned}\tilde{H}_{\text{eff}} = {} & \Delta_d m^\dagger m + \Delta_d \tilde{c}^\dagger \tilde{c} + \tilde{\xi} m \tilde{c}^\dagger + \tilde{\xi} \tilde{c} m^\dagger \\ & + \Omega_d(m^\dagger + m),\end{aligned} \tag{25}$$

where $\Delta_d = \omega_m - \omega_d$ is the magnon frequency from the driving field frequency.

Correspondingly, the master equation could be obtained by considering the dissipation of magnon and the decay rate of dressed atoms

$$\begin{aligned}\frac{d\rho}{dt} = {} & -i[\tilde{H}_{\text{eff}}, \rho] + \frac{\kappa_m}{2}(n_{\text{th}} + 1)\mathcal{L}[m] \\ & + \frac{\kappa_m}{2} n_{\text{th}} \mathcal{L}[m^\dagger] + \frac{\Gamma}{2}\mathcal{L}[\tilde{c}],\end{aligned} \tag{26}$$

wherein $\mathcal{L}[o]\rho = 2o\rho o^\dagger - o^\dagger o\rho - \rho o^\dagger o$ represents the Lindblad terms accounting for the environment losses.

As is well known, the magnon blockade effect is a typical quantum effect, which is a counterpart of Coulomb blockade and photon blockade [37,38]. For instance, the photon blockade describes such a phenomenon that the absorption of a photon by an arbitrary optical device will block the subsequent photon. Similarly, the magnon blockade effect can be described by evaluating the equal-time second-order correlation function [69],

$$g^{(2)}(0) = \frac{\langle m^\dagger m^\dagger m m\rangle_{ss}}{\langle m^\dagger m\rangle^2_{ss}}, \tag{27}$$

in which the symbol $\langle\cdots\rangle_{ss}$ represents the expectation value and $g^{(2)}(0)$ denotes the equal-time second-order correlation for magnon at steady state. For $g^{(2)}(0) > 1$, the correlation function illustrates that the super-Poisson distribution of magnon numbers is present, corresponding to magnon bunching. Otherwise, the magnon antibunching being related to sub-Poisson statistics is generated when $g^{(2)}(0) < 1$, implying the appearance of nonclassical effects. Especially, the perfect magnon blockade is obtained at $g^{(2)}(0) = 0$, which means the high-quality single-magnon source is possible to detect theoretically.

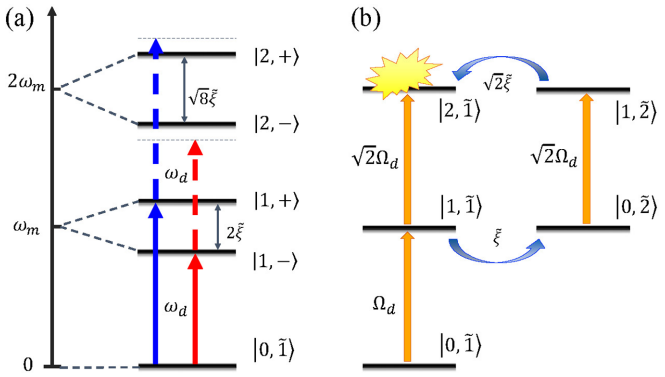

FIG. 7. (a) Energy-level diagram of the dressed states of the coupled system. Assuming the largest magnon excitation number n is equal to 2. (b) Energy-level diagram of the bare states of the system in the low-excitation subspace. The destructive interference between transition paths prevents the two-magnon excitation.

In general, the numerical results of the equal-time second-order correlation function could be easily derived from Eq. (26) by the way of QUTIP [82]. However, herein we would like to give an analytical result based on the perturbation theory. As usual, under the condition of weak driving field $\Omega_d \ll \Delta_d, \tilde{\xi}$, the reduced Hamiltonian (25) can be further diagonalized in the Hilbert space $|n,\tilde{1}\rangle, |n-1,\tilde{2}\rangle$, where $|n\rangle (n = 0, 1, 2, \ldots)$ denotes the number state of magnon. The corresponding eigenenergies are then given by

$$E_{n,\pm} = n\Delta_d \pm \tilde{\xi}\sqrt{n}. \tag{28}$$

It is easy to see that the energy splitting between states $|n,+\rangle$ and $|n,-\rangle$ is mainly determined by the following factors: the effective coherent coupling constant $g = g_a g_m/\Delta$, the amplitude ratio Ω_c/Ω_m and the magnon number n. Energy-level diagram of the dressed states of the coupled system is shown in Fig. 7(a). Accordingly, the magnon statistics property in our scheme can be conveniently controlled by the relative amplitude of the driving fields Ω_c/Ω_m.

To obtain the analytical result of second-order correlation function, one should solve the non-Hermitian Schrödinger equation by phenomenologically adding the dissipation rates of the system into the Hamiltonian $\tilde{H}_{\text{eff}}$, i.e.,

$$H'_{\text{non}} = \tilde{H}_{\text{eff}} - i\frac{\kappa_m}{2}m^\dagger m - i\frac{\Gamma}{2}\tilde{c}^\dagger\tilde{c}, \tag{29}$$

wherein the parameters κ_m and Γ are the dissipation rates of the magnon and atomic spin, respectively. By substituting the non-Hermitian Hamiltonian into

$$i\frac{\partial|\psi(t)}{\partial t} = H'_{\text{non}}|\psi(t), \tag{30}$$

where $|\psi(t)\rangle = \sum_{n=0}^{2} C_{n,\tilde{1}}|n,\tilde{1}\rangle + \sum_{m=0}^{1} C_{m,\tilde{2}}|m,\tilde{2}\rangle$. The parameters $C_{n,\tilde{1}}$ and $C_{m,\tilde{2}}$ represent the probability amplitudes for the states $|n,\tilde{1}\rangle$, $|m,\tilde{2}\rangle$, respectively. In the weak driving cases, the system would be confined into a low-excitation subspace. This leads to a fact that the magnon number state can be truncated into a two-magnon excitation subspace, thus the set of coupled equations of $C_{n,\tilde{1}}$ and $C_{m,\tilde{2}}$ is derived as

$$\begin{aligned}
0 &= \tilde{\Delta}_a C_{0,\tilde{2}} + \tilde{\xi} C_{1,\tilde{1}} + \Omega_d C_{1,\tilde{2}},\\
0 &= \tilde{\Delta}_m C_{1,\tilde{1}} + \tilde{\xi} C_{0,\tilde{2}} + \Omega_d C_{0,\tilde{1}} + \sqrt{2}\Omega_d C_{2,\tilde{1}},\\
0 &= (\tilde{\Delta}_a + \tilde{\Delta}_m) C_{1,\tilde{2}} + \Omega_d C_{0,\tilde{2}} + \sqrt{2}\tilde{\xi} C_{2,\tilde{1}},\\
0 &= \sqrt{2}\tilde{\xi} C_{1,\tilde{2}} + 2\tilde{\Delta}_m C_{2,\tilde{1}} + \sqrt{2}\Omega_d C_{1,\tilde{1}}
\end{aligned} \tag{31}$$

with $\tilde{\Delta}_a = \Delta_d - i\Gamma/2$, $\tilde{\Delta}_m = \Delta_d - i\kappa_m/2$. Under the fact of $C_{0,\tilde{1}} \simeq 1 \gg \{C_{1,\tilde{1}}, C_{0,\tilde{2}}\} \gg \{C_{2,\tilde{1}}, C_{1,\tilde{2}}\}$, one can give a concise expression for the steady-state second-order correlation function

$$g^{(2)}(0) \simeq \frac{2|C_{2,\tilde{1}}|^2}{|C_{1,\tilde{1}}|^4}. \tag{32}$$

Finally, the analytical results of $g^{(2)}(0)$ are given by

$$g^{(2)}(0) \simeq \frac{|\tilde{\xi}^2 - \tilde{\Delta}_a\tilde{\Delta}_m|^2|\tilde{\xi}^2 + \tilde{\Delta}_a(\tilde{\Delta}_a + \tilde{\Delta}_m)|^2}{|\tilde{\Delta}_a|^4|\tilde{\xi}^2 - \tilde{\Delta}_m(\tilde{\Delta}_a + \tilde{\Delta}_m)|^2}. \tag{33}$$

Obviously, $g^{(2)}(0)$ can take minimal values and the ideal magnon blockade may happen when $|\tilde{\xi}^2 - \tilde{\Delta}_a\tilde{\Delta}_m| \simeq 0$ or $\tilde{\xi}^2 + \tilde{\Delta}_a(\tilde{\Delta}_a + \tilde{\Delta}_m) = 0$. For the first case, under the strong coupling limit, $\tilde{\xi} \gg \{\kappa_m, \Gamma\}$, one can get the optimal conditions for the strong magnon antibunching effects as

$$\Delta_d \simeq= \pm\tilde{\xi} = \pm\frac{g\cos\theta}{2}\sqrt{N_1 - N_2}. \tag{34}$$

It is worthwhile to point out that the optimal conditions are exactly consistent with the energy splitting of the first excited states $|1,\pm\rangle$ in Eq. (28). This implies that the magnon mode is resonant with the transition from state $|0,\tilde{1}\rangle$ to the states $|1,\pm\rangle$, but is far detuned with the second transition from $|1,+\rangle(|1,-\rangle)$ to $|2,+\rangle(|2,-\rangle)$. Therefore, as shown in Fig. 7(a), the first magnon is absorbed followed by the inhibition of the successive one, which is the typical conventional magnon blockade (CMB) effects. Essentially, the strong energy splitting is created by the strong coupling $\tilde{\xi}$ between magnon and atom with indirect interactions. Being different from previous schemes [44,45,48], the coupling constant $\tilde{\xi}$ can be coherently controlled by the relative amplitude of driving fields. In fact, the parameter $\tilde{\xi}$ are equal to ξ for the two different cases of $\beta = \pm 1$. As shown in Fig. 5, it is obvious that the condition of $\tilde{\xi} \gg \{\kappa_m, \Gamma\}$ can be satisfied in the region of $0.3 \leqslant \Omega_c/\Omega_m \leqslant 0.62$.

In Fig. 8(a), logarithmic of the equal-time second-order correlation function $\log_{10}g^{(2)}(0)$ is plotted as a function of coupling constant g and amplitude ratio Ω_c/Ω_m under the condition of $\Delta_d \approx \tilde{\xi}$. To guarantee the validity for calculation of correlation function via perturbation theory, we only select the reliable region of $0.3 \leqslant \Omega_c/\Omega_m \leqslant 0.62$, in which we always have $\bar{N}_1 - \bar{N}_2 \approx 1$, as shown in Fig. 2(d). Figure 8(a) shows that the strong magnon antibunching $g^{(2)}(0)$ is generated in the nearly whole region. The larger coupling constant g is, the smaller the value of $g^{(2)}(0)$ is. It demonstrates that the ideal CMB is possible to happen within the strong and ultrastrong coupling regime. Besides, the strong magnon blockade becomes weak as the increasing of Ω_c/Ω_m, which can be observed more clearly from a two-dimensional curve in Fig. 8(b) by choosing different amplitude ratios $\Omega_c/\Omega_m = 0.3$ (solid

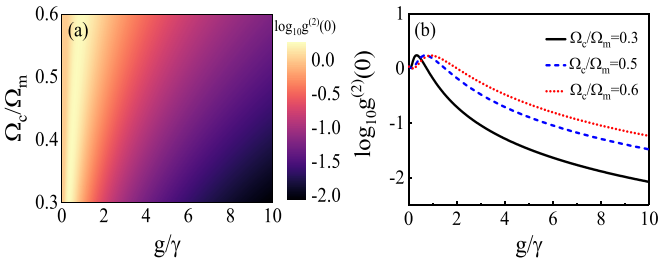

FIG. 8. (a) Logarithmic plot of the equal-time second-order correlation function $\log_{10}g^{(2)}(0)$ as a function of the coupling strength g/γ and the amplitude ratio Ω_c/Ω_m. (b) Logarithmic plot of the equal-time second-order correlation function $\log_{10}g^{(2)}(0)$ as a function of g/γ for different Ω_c/Ω_m. Taking parameters $\gamma_{1,2}=\gamma$, $\beta=-1$, $\kappa_m=0.1\gamma$, $\Omega_d=0.01\gamma$, $\gamma_p=0.01\gamma$, $\Delta_d=\tilde{\xi}$.

line), $\Omega_c/\Omega_m=0.5$ (dashed line), $\Omega_c/\Omega_m=0.6$ (dotted line). This can be attributed to the fact that the coupling strength $\tilde{\xi}$ is reduced with the increasing of Ω_c/Ω_m between 0.3 and 0.6, as shown in Fig. 5.

On the other hand, if $\tilde{\xi}^2+\tilde{\Delta}_a(\tilde{\Delta}_a+\tilde{\Delta}_m)=0$ has a nontrivial solution, we can obtain another condition for the optimal magnon antibunching as

$$\Delta_d\simeq 0,\quad g_{\rm opt}=\sec\theta\sqrt{\frac{\Gamma(\kappa_m+\Gamma)}{N_1-N_2}}. \tag{35}$$

In Fig. 9(a), we plot the logarithmic of $\log_{10}g^{(2)}(0)$ as a function of g and amplitude ratio Ω_c/Ω_m by setting $\Delta_d=0$. The parameters are the same as those in Fig. 8. Clearly, the magnon blockade only appears at some specific positions by appropriately choosing g and Ω_c/Ω_m, which is depicted by the white dashed line in Fig. 9(a). Similarly, in Fig. 9(b) we also plot the evolution of $\log_{10}g^{(2)}(0)$ versus g by choosing different amplitude ratios $\Omega_c/\Omega_m=0.3$ (solid line), $\Omega_c/\Omega_m=0.5$ (dashed line), $\Omega_c/\Omega_m=0.6$ (dotted line). It can be seen that the optimal value of g is $g_{\rm opt}=0.246\gamma$, $g_{\rm opt}=0.55\gamma$, $g_{\rm opt}=0.75\gamma$, respectively. In fact, based on Eq. (35), one can deduce directly that as the amplitude ratio increases, the population difference of N_1-N_2 is reduced, leading to the larger optimal values of $g_{\rm opt}$. Opposite to the first case, the magnon blockade

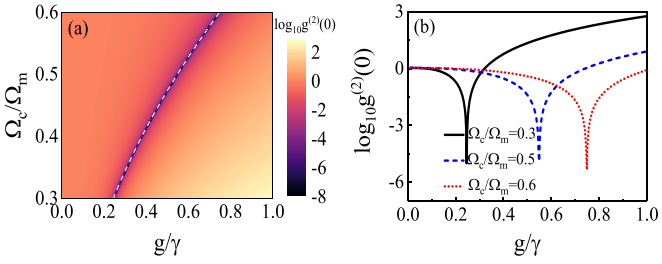

FIG. 9. (a) Logarithmic plot of the equal-time second-order correlation function $\log_{10}g^{(2)}(0)$ as a function of the coupling strength g/γ and the amplitude ratio Ω_c/Ω_m. (b) Logarithmic plot of the equal-time second-order correlation function $\log_{10}g^{(2)}(0)$ as a function of g/γ for different Ω_c/Ω_m. Setting $\Delta_d=0$, and the other parameters are the same as in Fig. 8. The white dashed line denotes the optimal condition described by Eq. (35).

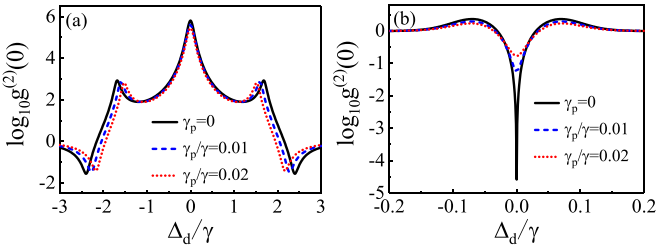

FIG. 10. Logarithmic plot of the equal-time second-order correlation function $\log_{10}g^{(2)}(0)$ as a function of Δ_d/γ for $\gamma_p=0$ (solid line), $\gamma_p=0.01\gamma$ (dashed line), $\gamma_p=0.02\gamma$ (dotted line). (a) $g=5\gamma$ and (b) $g=0.223\gamma$. Taking $\Omega_c/\Omega_m=0.3\gamma$ and the other parameters are the same as in Fig. 8.

is generated in the weak coupling region ($g<\gamma$). The internal mechanism is reasonably quite different from the first case. As shown in Fig. 7(b), there exist two different pathways to excite the magnon into the state $|2,\tilde{1}\rangle$, i.e., $|0,\tilde{1}\rangle\rightarrow|1,\tilde{1}\rangle\rightarrow|2,\tilde{1}\rangle$ and $|0,\tilde{1}\rangle\rightarrow|1,\tilde{1}\rangle\curvearrowright|0,\tilde{2}\rangle\rightarrow|1,\tilde{2}\rangle\curvearrowright|2,\tilde{1}\rangle$. It is the very quantum interference mechanism that gives rise to the occurrence of magnon blockade effect, which is named as unconventional magnon blockade (UCMB).

Moreover, it is of interest to discuss the effects of the other parameters on the CMB and UCMB. In the first of place, in Fig. 10, we plot the evolution of $\log_{10}g^{(2)}(0)$ as a function of Δ_d/γ by choosing different dephasing rate of $\gamma_p=0$ (solid line), $\gamma_p=0.01\gamma$ (dashed line), $\gamma_p=0.02\gamma$ (dotted line). The coupling constant is chosen as $g=5\gamma$ in Fig. 10(a) and $g=0.223\gamma$ in Fig. 10(b). The other parameters are the same as those in Fig. 8. When the dephasing rate is increased from $\gamma_p=0$ to $\gamma_p=0.02\gamma$, the optimal CMB appears at different Δ_d but the UCMB is always generated at $\Delta_d=0$. Meanwhile, the increase of the dephasing rate leads to the reduction of both CMB and UCMB. Physically, it is well known that coherent population trapping would be spoiled by the dephasing rate between the lower states of atoms, causing the reduction of magnon blockade. Furthermore, the dephasing rate has a more remarkable effect on UCMB. This is because the dephasing rate γ_p is detrimental to the quantum interference, as shown in Figs. 2(c) and 2(d), resulting in the obvious reduction of UCMB, which is originated from quantum interference between different pathways. In addition, we also concern on the influence of the dissipation rate of magnon κ_m on CMB and UCMB. Likewise, the increase of κ_m also leads to the reduction of both CMB and UCMB, as shown in Fig. 11. On the other hand, we find that the CMB and UCMB are robust against the experimental working temperature, which can be seen in Fig. 12. It should be noted that Fig. 12 is plotted by QUTIP [82]. For this reason, the numerical results shown in Fig. 12 are not completely consistent with the results in Fig. 10 based on the analytical method.

Finally, we would like to discuss the feasibility of the present scheme in experiment. Taking ^{87}Rb atoms as a potential candidate, the two ground states $|g_{1,2}\rangle$ are Zeeman sublevels of the same hyperfine state. As shown in Fig. 1, both the atoms and the YIG sphere are in the yz plane, and at the wave crest of the microwave field. The atoms are assumed to be trapped in a small volume [72]. A semiconductor laser can

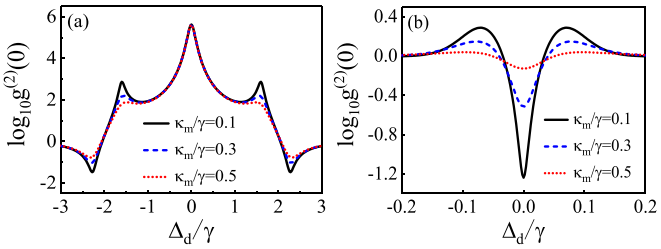

FIG. 11. Logarithmic plot of the equal-time second-order correlation function $\log_{10}g^{(2)}(0)$ as a function of Δ_d/γ for $\kappa_m = 0.1\gamma$ (solid line), $\kappa_m = 0.3\gamma$ (dashed line), $\kappa_m = 0.5\gamma$ (dotted line). Taking $\gamma_p = 0.01\gamma$ and the other parameters are the same as in Fig. 10.

supply the control field, which couples to the transition connecting the state $|g_2\rangle$ and excited state $|e\rangle$. Meanwhile, another resonant microwave field generated by a horn antennas [83] couples to transition $|g_1\rangle \leftrightarrow |g_2\rangle$ and travels in the x direction perpendicular to the CPWR. A coplanar waveguide resonator (CPWR) [72,84] can apply the microwave quantum field, which is simultaneously coupled with the atomic transition $|g_1\rangle \leftrightarrow |g_2\rangle$ and magnon mode with large detuning. In addition, similar to the present scheme, the quantum interference effects have been proposed in a three-state Λ system in which two Zeeman substates of the same hyperfine state constitute the two lower states [60].

On the other hand, it is worthwhile to note how to generate SGC in atomic or atomlike systems. Theoretically, the quantum interference effects are considered in the atomic system with near degenerate levels, i.e., the level space of the lower states satisfies the approximate condition of $\omega_{g_1g_2} \sim \gamma$ and with nonorthogonal dipole moments $\vec{\mu}_{eg_1}$ and $\vec{\mu}_{eg_2}$. The strength of the quantum interference is measured by the parameter β. In practice, it is a great challenge to find realistic atom with nonorthogonal dipole moments and quantum states close in energy [85]. In earlier literature, the experimental control of quantum interference has been observed in sodium dimers [86] but a conflicting result is reported later [87]. Fortunately, several theoretical and experimental approaches to overcome this restriction have been proposed successively. For instance, Agarwal *et al.* displayed that the anisotropy of the vacuum of the electromagnetic field can give rise to the generation of SGC effects without the requirement of nonorthogonal dipole moments [88]. Another different approach to verify the presence of spontaneous coherences is to use artificial atomic systems. It is reported that in charged GaAs quantum dots, the Raman spin coherence in the quantum beats is caused by the SGC effects with a three-level Λ-type configuration [66]. Kiffner *et al.* demonstrated that the conditions for SGC are indeed satisfied in a real four-level system in $J = 1/2 \leftrightarrow J = 1/2$ configuration [89]. Furthermore, it turns out that decay-induced cross couplings can be engineered via a suitable incoherent pumping [90]. Both three-level V and Λ systems may exhibit coherence effects even if they are driven with incoherent fields only. In recent years, Brumer *et al.* pay continuous interest to investigate the generation of noise-induced quantum coherences beyond the secular approximation and an experimental proposal is suggested [67,68]. In a word, the SGC effects can be verified with various methods and can be observed in experiment.

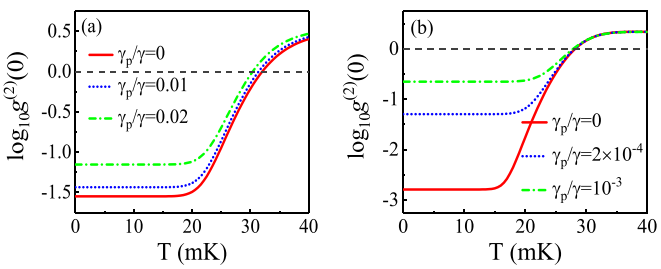

FIG. 12. Logarithmic plot of the equal-time second-order correlation function $\log_{10}g^{(2)}(0)$ versus temperature T for different dephasing rates. Taking $\omega_m/2\pi = 6.5$ GHz and the other parameters are the same as in Fig. 10.

Before ending this section, we would like to emphasis the main results found in the present scheme. First, by utilizing the quantum interference in spontaneous generation and the atomic coherence induced by the strong fields, we propose a scheme to realize the switching of anti-JC interaction and JC interaction, resulting in the generation of entanglement and blockade, respectively. Second, we find that the coherent coupling between atoms and magnon is established via virtual photon exchange when the cavity field is tuned to be far detuned with the atomic transition and magnons [34], simultaneously. The quantum entanglement and magnon blockade can be conveniently controlled by the relative intensity of the driven fields. Third, we consider the effect of dephasing rate on entanglement and blockade, showing that these quantum effects are still generated when the atomic decoherence rate is introduced [91]. In addition, it is noted that our results are also robust against the magnon dissipation rate and thermal environment noise, relatively.

V. CONCLUSION

In conclusion, we suggest a scheme to realize the magnon-atom entanglement and magnon blockade based on the quantum interference together with atomic coherence in a hybrid magnon-cavity-atom system. By placing a three-level Λ-type atomic ensemble and a YIG sphere into a microwave cavity, when two strong fields are applied to resonantly drive the atomic system, it is demonstrated that the coherent coupling between the atoms and magnon without direct interaction is established in dressed-state picture through virtual photon exchange. Of great interest, the anti-JC-type and JC-type interactions are alternatively formed when the two dipole moments of atoms are parallel or antiparallel, which leads to the appearance of hybrid magnon-atom entanglement and magnon blockade. We show that the good entanglement and magnon blockade are strongly dependent on the relative amplitude of the two strong driving fields. This provides an effective way to control quantum effects and may find potential applications in quantum information processing.

ACKNOWLEDGMENT

This work is supported by the National Natural Science Foundation of China (Grant No. 11574179) and is funded

by the National "111 Research Center" Microelectronics Circuits.

APPENDIX: DRESSED ATOMIC POPULATIONS

The atomic damping term in Eq. (7) is written in terms of the dressed atomic states in an explicit form

$$\mathcal{L}_a\widetilde{\rho} = \sum_{j,k=\tilde{0},\tilde{1},\tilde{2}}^{j\neq k}\left(\mathcal{L}_{kj}^{jk}\widetilde{\rho} + \mathcal{L}_{kj}^{\mathrm{ph}}\widetilde{\rho}\right) + \sum_{j,k=\tilde{1},\tilde{2}}^{j\neq k}\mathcal{L}_{kj}^{\mathrm{in}}\widetilde{\rho}, \tag{A1}$$

where

$$\begin{aligned}
\mathcal{L}_{kj}^{jk}\widetilde{\rho} &= \frac{\gamma_{jk}}{2}(2\sigma_{jk}\widetilde{\rho}\sigma_{kj} - \sigma_{kj}\sigma_{jk}\widetilde{\rho} - \widetilde{\rho}\sigma_{kj}\sigma_{jk}),\\
\mathcal{L}_{kj}^{\mathrm{ph}}\widetilde{\rho} &= \frac{\gamma_{kj}^{\mathrm{ph}}}{4}\left(2\sigma_p^{kj}\widetilde{\rho}\sigma_p^{kj} - \sigma_p^{kj}\sigma_p^{kj}\widetilde{\rho} - \widetilde{\rho}\sigma_p^{kj}\sigma_p^{kj}\right),\\
\mathcal{L}_{kj}^{\mathrm{in}}\widetilde{\rho} &= \gamma_{kj}^{c}(\sigma_{j0}\widetilde{\rho}\sigma_{k0} + \sigma_{0k}\widetilde{\rho}\sigma_{0j})
\end{aligned} \tag{A2}$$

with $\sigma_p^{kj} = \sigma_{kk} - \sigma_{jj}$. The parameters in the above expressions are

$$\begin{aligned}
\gamma_{\tilde{0}\tilde{2}} &= \gamma_{\tilde{0}\tilde{1}} = \frac{\gamma_1\sin^4\theta}{2} + \frac{\gamma_p\sin^2 2\theta}{16},\\
\gamma_{\tilde{2}\tilde{0}} &= \frac{\gamma_1\cos^4\theta}{2} + \frac{\gamma_2\cos^2\theta}{2} + \frac{\gamma_p\sin^2 2\theta}{16} + \gamma_{12}\cos^3\theta,\\
\gamma_{\tilde{1}\tilde{0}} &= \frac{\gamma_1\cos^4\theta}{2} + \frac{\gamma_2\cos^2\theta}{2} + \frac{\gamma_p\sin^2 2\theta}{16} - \gamma_{12}\cos^3\theta,\\
\gamma_{\tilde{2}\tilde{1}} &= \frac{\gamma_1\sin^2 2\theta}{16} + \frac{\gamma_2\sin^2\theta}{4} + \frac{\gamma_p(\cos^2\theta+1)^2}{8}\\
&\quad + \frac{\gamma_{12}\sin^2\theta\cos\theta}{2},\\
\gamma_{\tilde{1}\tilde{2}} &= \frac{\gamma_1\sin^2 2\theta}{16} + \frac{\gamma_2\sin^2\theta}{4}\\
&\quad + \frac{\gamma_p(\cos^2\theta+1)^2}{8} - \frac{\gamma_{12}\sin^2\theta\cos\theta}{2},\\
\gamma_{\tilde{0}\tilde{2}}^{\mathrm{ph}} &= \frac{\gamma_1\sin^2 2\theta}{4} + \frac{\gamma_p\sin^4\theta}{2} + \gamma_{12}\sin^2\theta\cos\theta,\\
\gamma_{\tilde{0}\tilde{1}}^{\mathrm{ph}} &= \frac{\gamma_1\sin^2 2\theta}{4} + \frac{\gamma_p\sin^4\theta}{2} - \gamma_{12}\sin^2\theta\cos\theta,\\
\gamma_{\tilde{2}\tilde{1}}^{\mathrm{ph}} &= -\frac{\gamma_1\sin^2 2\theta}{8} + \frac{\gamma_2\sin^2\theta}{2} - \frac{\gamma_p\sin^4\theta}{4},\\
\gamma_{\tilde{2}\tilde{1}}^{c} &= -\frac{\gamma_1\sin^2 2\theta}{8} + \frac{\gamma_p\sin^2 2\theta}{16} + \frac{\gamma_{12}\sin^2\theta\cos\theta}{2},\\
\gamma_{\tilde{1}\tilde{2}}^{c} &= -\frac{\gamma_1\sin^2 2\theta}{8} + \frac{\gamma_p\sin^2 2\theta}{16} - \frac{\gamma_{12}\sin^2\theta\cos\theta}{2}.
\end{aligned} \tag{A3}$$

Neglecting the quantized modes temporarily, we can obtain the steady-state populations of the dressed states

$$\begin{aligned}
N_0 &= N\frac{\gamma_{\tilde{0}\tilde{1}}\gamma_{\tilde{1}\tilde{2}} + (\gamma_{\tilde{0}\tilde{1}} + \gamma_{\tilde{2}\tilde{1}})\gamma_{\tilde{0}\tilde{2}}}{D},\\
N_1 &= N\frac{\gamma_{\tilde{1}\tilde{2}}\gamma_{\tilde{2}\tilde{0}} + (\gamma_{\tilde{0}\tilde{2}} + \gamma_{\tilde{1}\tilde{2}})\gamma_{\tilde{1}\tilde{0}}}{D},\\
N_2 &= N\frac{\gamma_{\tilde{1}\tilde{0}}\gamma_{\tilde{2}\tilde{1}} + (\gamma_{\tilde{0}\tilde{1}} + \gamma_{\tilde{2}\tilde{1}})\gamma_{\tilde{2}\tilde{0}}}{D},
\end{aligned} \tag{A4}$$

where N_0, N_1, N_2 represent the steady-state populations of the dressed states, and $D = \gamma_{\tilde{1}\tilde{0}}(\gamma_{\tilde{1}\tilde{2}} + \gamma_{\tilde{0}\tilde{2}} + \gamma_{\tilde{2}\tilde{1}}) + \gamma_{\tilde{1}\tilde{2}}(\gamma_{\tilde{0}\tilde{1}} + \gamma_{\tilde{2}\tilde{0}}) + (\gamma_{\tilde{0}\tilde{1}} + \gamma_{\tilde{2}\tilde{1}})(\gamma_{\tilde{0}\tilde{2}} + \gamma_{\tilde{2}\tilde{0}})$. The decay rate of the spin down flip operator can be derived as

$$\Gamma = 2\gamma_{\tilde{2}\tilde{1}}^{\mathrm{ph}} + \tfrac{1}{2}\left(\gamma_{\tilde{0}\tilde{2}}^{\mathrm{ph}} + \gamma_{\tilde{0}\tilde{1}}^{\mathrm{ph}}\right) + \gamma_{\tilde{2}\tilde{1}} + \gamma_{\tilde{1}\tilde{2}} + \gamma_{\tilde{0}\tilde{2}} + \gamma_{\tilde{0}\tilde{1}}. \tag{A5}$$

[1] X. Zhang, C.-L. Zou, L. Jiang, and H. X. Tang, Phys. Rev. Lett. **113**, 156401 (2014).

[2] Y. P. Wang, G. Q. Zhang, D. Zhang, X. Q. Luo, W. Xiong, S. P. Wang, T. F. Li, C. M. Hu, and J. Q. You, Phys. Rev. B **94**, 224410 (2016).

[3] J. Bourhill, N. Kostylev, M. Goryachev, D. L. Creedon, and M. E. Tobar, Phys. Rev. B **93**, 144420 (2016).

[4] N. Kostylev, M. Goryachev, and M. E. Tobar, Appl. Phys. Lett. **108**, 062402 (2016).

[5] X. Zhang, N. Zhu, C.-L. Zou, and H. X. Tang, Phys. Rev. Lett. **117**, 123605 (2016).

[6] J. A. Haigh, A. Nunnenkamp, A. J. Ramsay, and A. J. Ferguson, Phys. Rev. Lett. **117**, 133602 (2016).

[7] A. Osada, R. Hisatomi, A. Noguchi, Y. Tabuchi, R. Yamazaki, K. Usami, M. Sadgrove, R. Yalla, M. Nomura, and Y. Nakamura, Phys. Rev. Lett. **116**, 223601 (2016).

[8] A. A. Serga, A. V. Chumak, and B. Hillebrands, J. Phys. D **43**, 264002 (2010).

[9] M. Goryachev, W. G. Farr, D. L. Creedon, Y. Fan, M. Kostylev, and M. E. Tobar, Phys. Rev. Appl. **2**, 054002 (2014).

[10] D. Zhang, X. M. Wang, T. F. Li, X. Q. Luo, W. Wu, F. Nori, and J. Q. You, npj Quantum Inf. **1**, 15014 (2015).

[11] T. Niemczyk, F. Deppe, H. Huebl, E. Menzel, F. Hocke, M. Schwarz, J. Garcia-Ripoll, D. Zueco, T. Hümmer, E. Solano *et al.*, Nature Phys. **6**, 772 (2010).

[12] J. A. Haigh, S. Langenfeld, N. J. Lambert, J. J. Baumberg, A. J. Ramsay, A. Nunnenkamp, and A. J. Ferguson, Phys. Rev. A **92**, 063845 (2015).

[13] A. Osada, A. Gloppe, R. Hisatomi, A. Noguchi, R. Yamazaki, M. Nomura, Y. Nakamura, and K. Usami, Phys. Rev. Lett. **120**, 133602 (2018).

[14] T. S. Parvini, V. A. S. V. Bittencourt, S. V. Kusminskiy, Phys. Rev. Res. **2**, 022027(R) (2020).

[15] X. Zhang, C.-L. Zou, L. Jiang, and H. X. Tang, Sci. Adv. **2**, e1501286 (2016).

[16] C. A. Potts, E. Varga, V. A. S. V. Bittencourt, S. V. Kusminskiy, and J. P. Davis, Phys. Rev. X **11**, 031053 (2021).

[17] Y. Tabuchi, S. Ishino, A. Noguchi, T. Ishikawa, R. Yamazaki, K. Usami, and Y. Nakamura, Science **349**, 405 (2015); C. R. Phys. **17**, 729 (2016).

[18] A. Clerk, K. Lehnert, P. Bertet, J. Petta, and Y. Nakamura, Nature Phys. **16**, 257 (2020).

[19] D. Lachance-Quirion, Y. Tabuchi, A. Gloppe, K. Usami, and Y. Nakamura, Appl. Phys. Express **12**, 070101 (2019).

[20] Y.-P. Wang, G.-Q. Zhang, D. Zhang, T.-F. Li, C.-M. Hu, and J. Q. You, Phys. Rev. Lett. **120**, 057202 (2018).

[21] Z. Zhang, M. O. Scully, and G. S. Agarwal, Phys. Rev. Res. **1**, 023021 (2019).

[22] R. C. Shen, Y. P. Wang, J. Li, S.-Y. Zhu, G. S. Agarwal, and J. Q. You, Phys. Rev. Lett. **127**, 183202 (2021).

[23] K. Ullah, M. T. Naseen, and Ö. E. Müstecaplıoğlu, Phys. Rev. A **102**, 033721 (2020).
[24] B. Wang, Z.-X. Liu, C. Kong, H. Xiong, and Y. Wu, Opt. Express **26**, 20248 (2018).
[25] Y. Iguchi, S. Uemura, K. Ueno, and Y. Onose, Phys. Rev. B **92**, 184419 (2015).
[26] C. Kong, H. Xiong, and Y. Wu, Phys. Rev. Appl. **12**, 034001 (2019).
[27] Z. Liu, H. Xiong, and Y. Wu, IEEE Access **7**, 57047 (2019).
[28] C. Kong, B. Wang, Z.-X. Liu, H. Xiong, and Y. Wu, Opt. Express **27**, 5544 (2019).
[29] J. Li, S.-Y. Zhu, and G. S. Agarwal, Phys. Rev. A **99**, 021801(R) (2019).
[30] H. Y. Yuan, P. Yan, S. Zheng, Q. Y. He, K. Xia, and M.-H. Yung, Phys. Rev. Lett. **124**, 053602 (2020).
[31] S. Sharma, V. A. S. V. Bittencourt, A. D. Karenowska, and S. V. Kusminskiy, Phys. Rev. B **103**, L100403 (2021).
[32] F.-X. Sun, S.-S. Zheng, Y. Xiao, Q. Gong, Q. He, and K. Xia, Phys. Rev. Lett. **127**, 087203 (2021).
[33] J. Li, S.-Y. Zhu, and G. S. Agarwal, Phys. Rev. Lett. **121**, 203601 (2018).
[34] D. Y. Kong, X. M. Hu, L. Hu, and J. Xu, Phys. Rev. B **103**, 224416 (2021).
[35] E. T. Jaynes and F. W. Cummings, Proc. IEEE **51**, 89 (1963).
[36] B. W. Shore and P. L. Knight, J. Mod. Opt. **40**, 1195 (1993).
[37] K. M. Birnbaum, A. Boca, R. Miller, A. D. Boozer, T. E. Northup, and H. J. Kimble, Nature (London) **436**, 87 (2005).
[38] A. Nunnenkamp, K. Borkje, and S. M. Girvin, Phys. Rev. Lett. **107**, 063602 (2011).
[39] Z. Yuan, B. E. Kardynal, R. M. Stevenson, A. J. Shields, C. J. Lobo, K. Cooper, N. S. Beattie, D. A. Ritchie, and M. Pepper, Science **295**, 102 (2002).
[40] A. Kuhn, M. Hennrich, and G. Rempe, Phys. Rev. Lett. **89**, 067901 (2002).
[41] P. Rabl, Phys. Rev. Lett. **107**, 063601 (2011).
[42] J. Li, C. Ding, and Y. Wu, Phys. Rev. A **100**, 033814 (2019).
[43] S. Rosenblum, S. Parkins, and B. Dayan, Phys. Rev. A **84**, 033854 (2011).
[44] Z. X. Liu, H. Xiong, and Y. Wu, Phys. Rev. B **100**, 134421 (2019).
[45] J.-K. Xie, S.-L. Ma, and F.-L. Li, Phys. Rev. A **101**, 042331 (2020).
[46] Y.-J. Xu, T.-L. Yang, L. Lin, and J. Song, J. Opt. Soc. Am. B **38**, 876 (2021).
[47] C. S. Zhao, X. Li, S. L. Chao, R. Peng, and C. Li, L. Zhou, Phys. Rev. A **101**, 063838 (2020).
[48] K. Wu, W. X. Zhong, G.-L. Cheng, and A. X. Chen, Phys. Rev. A **103**, 052411 (2021).
[49] M. D. Lukin, Rev. Mod. Phys. **75**, 457 (2003).
[50] H. Xiong, M. O. Scully, and M. S. Zubairy, Phys. Rev. Lett. **94**, 023601 (2005).
[51] X. M. Hu, Phys. Rev. A **92**, 022329 (2015).
[52] S. L. Braunstein and H. J. Kimble, Phys. Rev. Lett. **80**, 869 (1998).
[53] X. Y. Li, Q. Pan, J. T. Jing, J. Zhang, C. D. Xie, and K. C. Peng, Phys. Rev. Lett. **88**, 047904 (2002).
[54] S. Lloyd and S. L. Braunstein, Phys. Rev. Lett. **82**, 1784 (1999).
[55] G. S. Agarwal, *Quantum Optics*, Springer Tracts in Modern Physics (Springer-Verlag, Berlin, 1974), Vol. 70.
[56] P. Zhou and S. Swain, Phys. Rev. Lett. **77**, 3995 (1996).
[57] S. Y. Zhu and M. O. Scully, Phys. Rev. Lett. **76**, 388 (1996).
[58] H. T. Tan, H. X. Xia, and G. X. Li, Phys. Rev. A **79**, 063805 (2009).
[59] K. E. Dorfman, P. K. Jha, and S. Das, Phys. Rev. A **84**, 053803 (2011).
[60] J. Javanainen, Europhys. Lett. **17**, 407 (1992).
[61] S. Menon and G. S. Agarwal, Phys. Rev. A **57**, 4014 (1998).
[62] J. H. Wu and J. Y. Gao, Phys. Rev. A **65**, 063807 (2002).
[63] A. Joshi, W. Yang, and X. Xiao, Phys. Lett. A **315**, 203 (2003).
[64] J. Evers, D. Bullock, and C. H. Keitel, Opt. Commun. **209**, 173 (2002).
[65] I. Gonzalo, M. A. Antón, F. Carreño, and O. G. Calderón, Phys. Rev. A **72**, 033809 (2005).
[66] M. V. G. Dutt *et al.*, Phys. Rev. Lett. **94**, 227403 (2005).
[67] T. V. Tscherbul and P. Brumer, Phys. Rev. Lett. **113**, 113601 (2014).
[68] A. Dodin, T. Tscherbul, R. Alicki, A. Vutha, and P. Brumer, Phys. Rev. A **97**, 013421 (2018).
[69] D. F. Walls and G. J. Milburn, *Quantum Optics* (Springer-Verlag, Berlin, 1994).
[70] M. O. Scully and M. S. Zubairy, *Quantum Optics* (Cambridge University Press, Cambridge, 1997).
[71] C. Cohen-Tannoudji, J. Dupont-Roc, and G. Grynberg, *Atom-photon Interactions* (Wiley, New York, 1992).
[72] D. Petrosyan, G. Bensky, G. Kurizki, I. Mazets, J. Majer, and J. Schmiedmayer, Phys. Rev. A **79**, 040304(R) (2009).
[73] H. Li, V. A. Sautenkov, Y. V. Rostovtsev, G. R. Welch, P. R. Hemmer, and M. O. Scully, Phys. Rev. A **80**, 023820 (2009).
[74] C. Hamsen, K. N. Tolazzi, T. Wilk, and G. Rempe, Nature Phys. **14**, 885 (2018).
[75] D. F. V. James, Fortschr. Phys. **48**, 823 (2000).
[76] T. Holstein and H. Primakoff, Phys. Rev. **58**, 1098 (1940).
[77] C. W. Gardiner and P. Zoller, *Quantum Noise*, 2nd ed. (Springer, Berlin, 2000).
[78] E. X. DeJesus and C. Kaufman, Phys. Rev. A **35**, 5288 (1987).
[79] D. Vitali, S. Gigan, A. Ferreira, H. R. Bohm, P. Tombesi, A. Guerreiro, V. Vedral, A. Zeilinger, and M. Aspelmeyer, Phys. Rev. Lett. **98**, 030405 (2007).
[80] G. Vidal and R. F. Werner, Phys. Rev. A **65**, 032314 (2002).
[81] M. B. Plenio, Phys. Rev. Lett. **95**, 090503 (2005).
[82] J. R. Johansson, P. D. Nation, and F. Nori, Comput. Phys. Commun. **184**, 1234 (2013).
[83] J. Han, T. Vogt, C. Gross, D. Jaksch, M. Kiffner, and W. Li, Phys. Rev. Lett. **120**, 093201 (2018).
[84] J. Verdu, H. Zoubi, Ch. Koller, J. Majer, H. Ritsch, and J. Schmiedmayer, Phys. Rev. Lett. **103**, 043603 (2009).
[85] Z. Ficek and S. Swain, J. Mod. Opt. **49**, 3 (2002).
[86] H. R. Xia, C. Y. Ye, and S. Y. Zhu, Phys. Rev. Lett. **77**, 1032 (1996).
[87] L. Li, X. Wang, J. Yang, G. Lazarov, J. Qi, and A. M. Lyyra, Phys. Rev. Lett. **84**, 4016 (2000).
[88] G. S. Agarwal and A. K. Patnaik, Phys. Rev. A **63**, 043805 (2001).
[89] M. Kiffner, J. Evers, and C. H. Keitel, Phys. Rev. Lett. **96**, 100403 (2006).
[90] G. C. Hegerfeldt and M. B. Plenio, Phys. Rev. A **47**, 2186 (1993).
[91] J. Xu and F. Wang, Phys. Rev. A **104**, 013706 (2021).